

Additive Manufacturing of Nickel-Base Superalloy IN100 Through Scanning Laser Epitaxy

AMRITA BASAK¹ and SUMAN DAS^{1,2,3}

1.—George W. Woodruff School of Mechanical Engineering, Georgia Institute of Technology, 801 Ferst Drive, Atlanta, GA 30332, USA. 2.—School of Materials Science and Engineering, Georgia Institute of Technology, 771 Ferst Drive NW, Atlanta, GA 30313, USA. 3.—e-mail: sumandas@gatech.edu

Scanning laser epitaxy (SLE) is a laser powder bed fusion (LPBF)-based additive manufacturing process that uses a high-power laser to consolidate metal powders facilitating the fabrication of three-dimensional objects. In the present study, SLE is used to produce samples of IN100, a high- γ' non-weldable nickel-base superalloy on similar chemistry substrates. A thorough analysis is performed using various advanced material characterization techniques such as high-resolution optical microscopy, scanning electron microscopy, energy dispersive x-ray spectroscopy, and Vickers microhardness measurements to characterize and compare the quality of the SLE-fabricated IN100 deposits with the investment cast IN100 substrates. The results show that the IN100 deposits have a finer γ/γ' microstructure, weaker elemental segregation, and higher microhardness compared with the substrate. Through this study, it is demonstrated that the SLE process has tremendous potential in the repair and manufacture of gas turbine hot-section components.

INTRODUCTION

Nickel-base superalloys are extensively used in aircraft and power-generation turbines, rocket engines, and other challenging high-temperature environments as these alloys offer higher yield strength with increasing operating temperatures under aggressive loading scenarios. Over the past few decades, extensive research into superalloy development has culminated in the productionization of components that can withstand up to 90% of the melting temperature of the material.¹ However, in nickel-base superalloys, precipitation of the γ' phases causes strain age cracking, hardening of the alloy during thermal exposure, and transfer of the solidification strains onto the grain boundaries.¹ The susceptibility to strain age cracking and alloy weldability for nickel-base superalloys is often qualitatively described by calculating the aluminum (Al) and titanium (Ti) content in the alloys.² An alloy is considered non-weldable if the total Al + Ti content exceeds 4 wt.%.²

The total Al + Ti content for IN100 is 11.0 wt.%. Hence, it is considered to be one of the most difficult-to-weld alloys. As a result, limited research is

available on welding or additive processing of this alloy system.³ The micro-laser aided additive manufacturing (micro-LAAM) process showed successful depositions of IN100 on cast IN100 substrates.⁴ This process, however, showed limitations with regard to the deposit thickness because of low laser power. In contrast, the scanning laser epitaxy (SLE) process demonstrated the fabrication of more than 1000 μm thick IN100 deposits on investment cast IN100 substrates in a single pass.⁵ Apart from IN100, the SLE process has shown encouraging results for one-step repair of several popular hot-section superalloys such as René 80,⁶ MAR-M247,⁷ René 142,⁸ CMSX-4[®],^{9–12} and René N5.^{13,14} A thorough review on the additive manufacturing (AM)-based processing of nickel-base superalloys may be found elsewhere and is skipped here for brevity.^{3,15}

Higher content of lighter elements such as Al and Ti and lower content of heavier elements such as refractory metals make IN100 particularly attractive on the basis of the strength-to-density ratio. IN100 has been extensively used in the fabrication of turbine blades, vanes, and nozzles in the gas turbine engines. The alloy has a nominal density of 7750 kg/m³ with a melting range of 1260–1335 °C.

IN100 exhibits excellent performance during cyclic testing, and after 200 h with 16 h of heating and 8 h of cooling cycle, the alloy showed only a 0.8% change in weight.¹⁶ In the present study, multiple samples of IN100 are produced through SLE, a laser-powder bed fusion (LPBF)-based AM process. The microstructure and the microhardness properties of the as-deposited IN100 and the investment cast IN100 substrates were investigated using high-resolution optical microscopy (HR-OM),

scanning electron microscopy (SEM), energy dispersive x-ray spectroscopy (EDS), and Vickers microhardness measurements, and the results are reported.

EXPERIMENTAL

A single-mode 1 kW Ytterbium fiber-laser (IPG Photonics, model: YLS-1000) was used in the present study. A three-axis galvanometer scanning

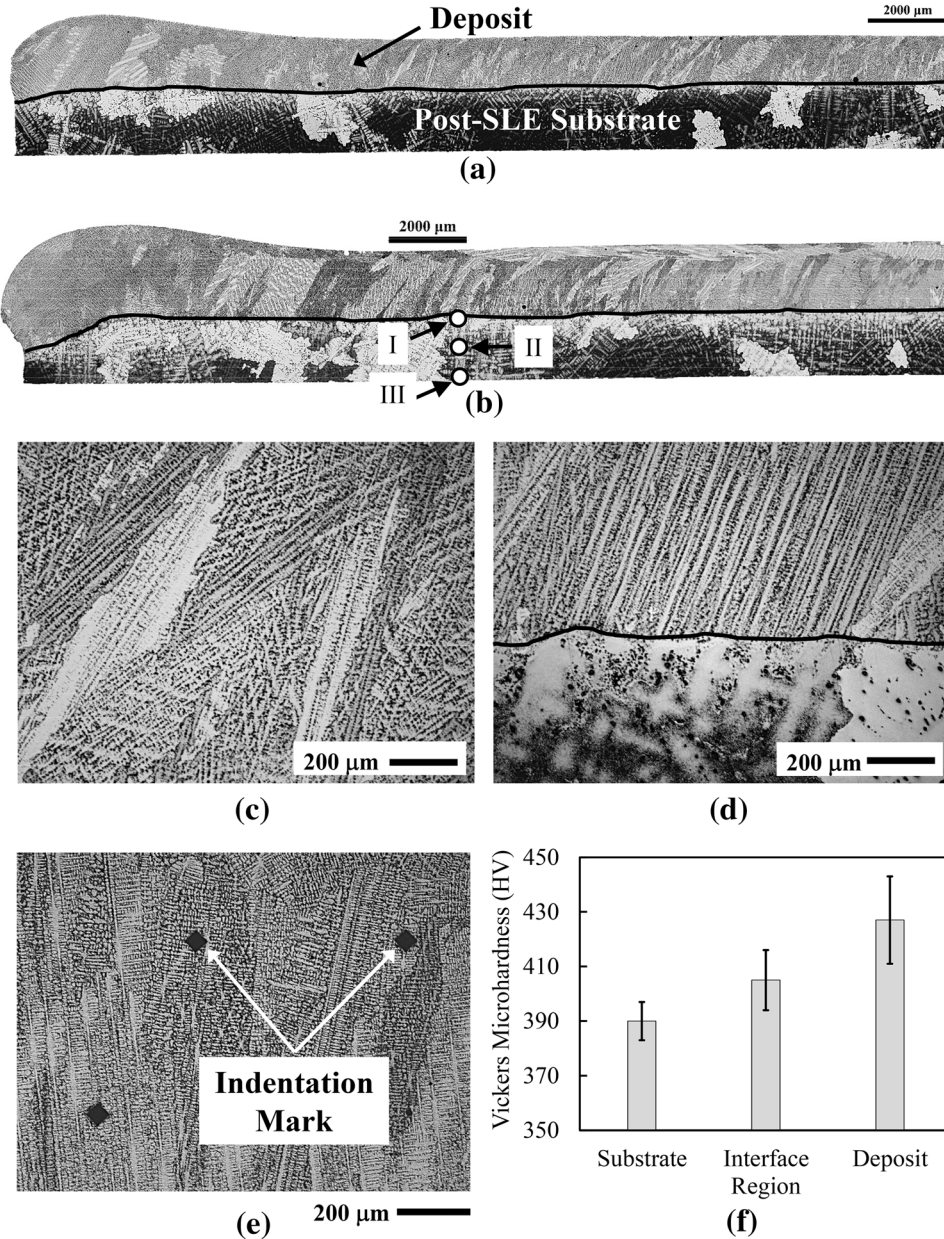


Fig. 1. HR-OM image of the SLE-deposited IN100 on IN100 substrate for (a) Sample 1 and (b) Sample 2. (c) IN100 microstructure in the deposit region and (d) the metallurgical bond between the substrate and the deposit. The black line in (a), (b), and (d) represents the interface between the deposit and the post-SLE substrate regions. (e) Representative indentation marks in the IN100 deposit and (f) variation in microhardness.

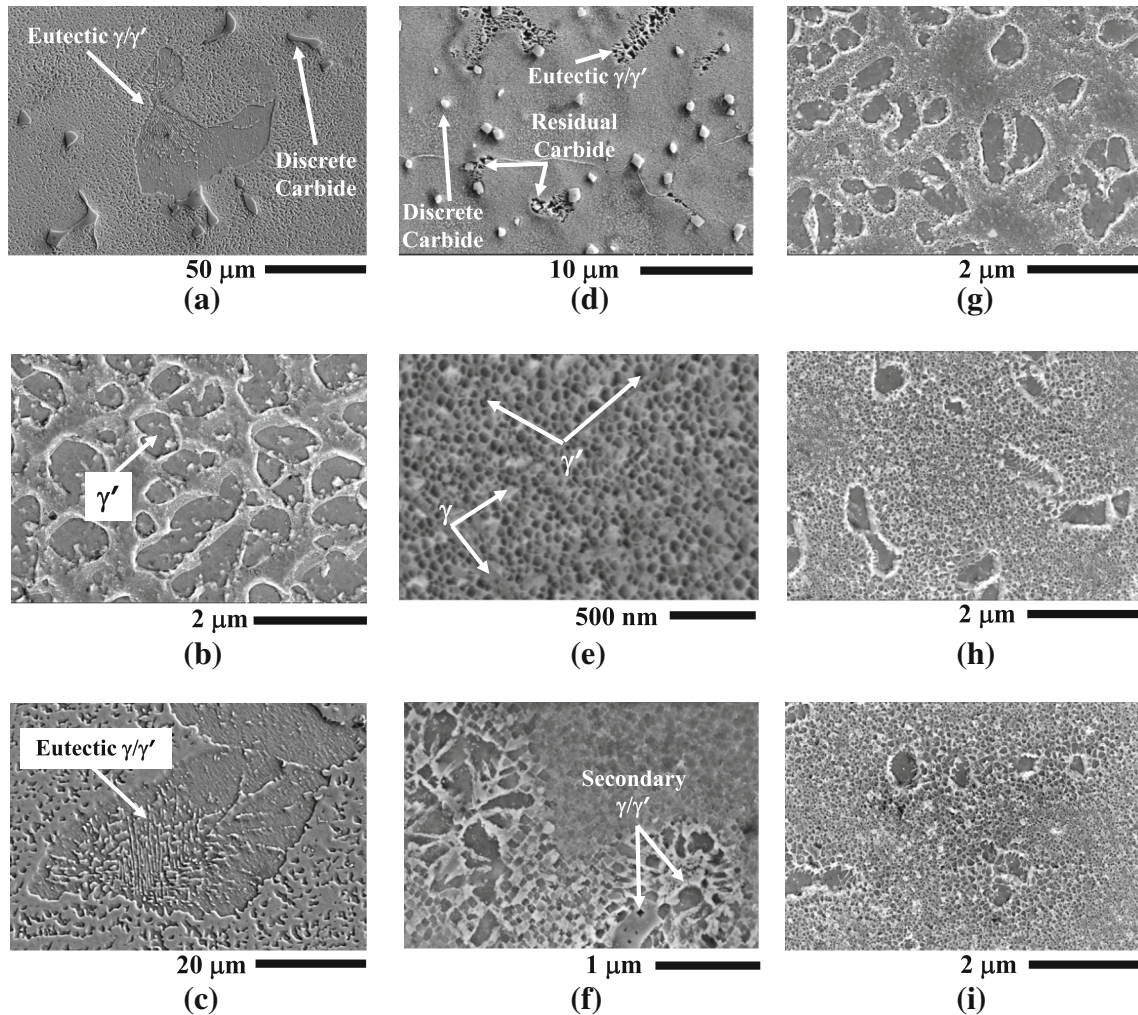


Fig. 2. SEM image of (a) the major constituents, (b) the γ/γ' structure, and (c) the eutectic region in the substrate. SEM image of (d) the major constituents, (e) the γ/γ' structure, and (f) the eutectic region in the deposit. SEM image of the γ/γ' structure in the post-SLE substrate at (g) Location III, (h) Location II, and (i) Location I of Fig. 1b.

system (Cambridge Technology) was used to direct the laser on top of the substrate and to focus the laser beam to a Gaussian beam diameter of $40\ \mu\text{m}$. This enabled tight control of the energy density within the melt pool. The SLE process was carried out on rectangular equiaxed (EQ) cast IN100 substrate coupons with dimensions of $35.56\ \text{mm} \times 6.86\ \text{mm} \times 2.54\ \text{mm}$. Argon gas-atomized IN100 powder produced by Pratt & Whitney—HMI Metal Powders (Clayville, NY) was used in this study.⁵ Hereafter, the substrate coupon after the SLE processing is referred to as a “post-SLE substrate coupon.” The substrate with the pre-placed powder fused to it after SLE processing is referred to as a “sample.” Details on experimental procedure, sample preparation, microstructure characterization, and microhardness measurements are found elsewhere and skipped here for brevity.^{5-7,11}

RESULTS AND DISCUSSION

SLE-Processed Microstructure and Vickers Microhardness

The longitudinal cross-sections of two representative IN100 samples (Sample 1 and Sample 2) are shown in Fig. 1a and b. Results from a previously established design-of-experiments (DoE) based method were used to make the substrate–deposit interface and the deposit height nearly flat.⁵ The deposit thickness was found to be of order $1300\ \mu\text{m}$ for Sample 1 and $1700\ \mu\text{m}$ for Sample 2.⁵ As illustrated in Fig. 1a and b, the deposit was crack-free and dense and continuously bonded to the substrate along the entire length of the substrate without any interface fusion defects.

As shown in Fig. 1a and b, an insignificant number of pores was observed in the deposit region. A DoE-based optimization study demonstrated that

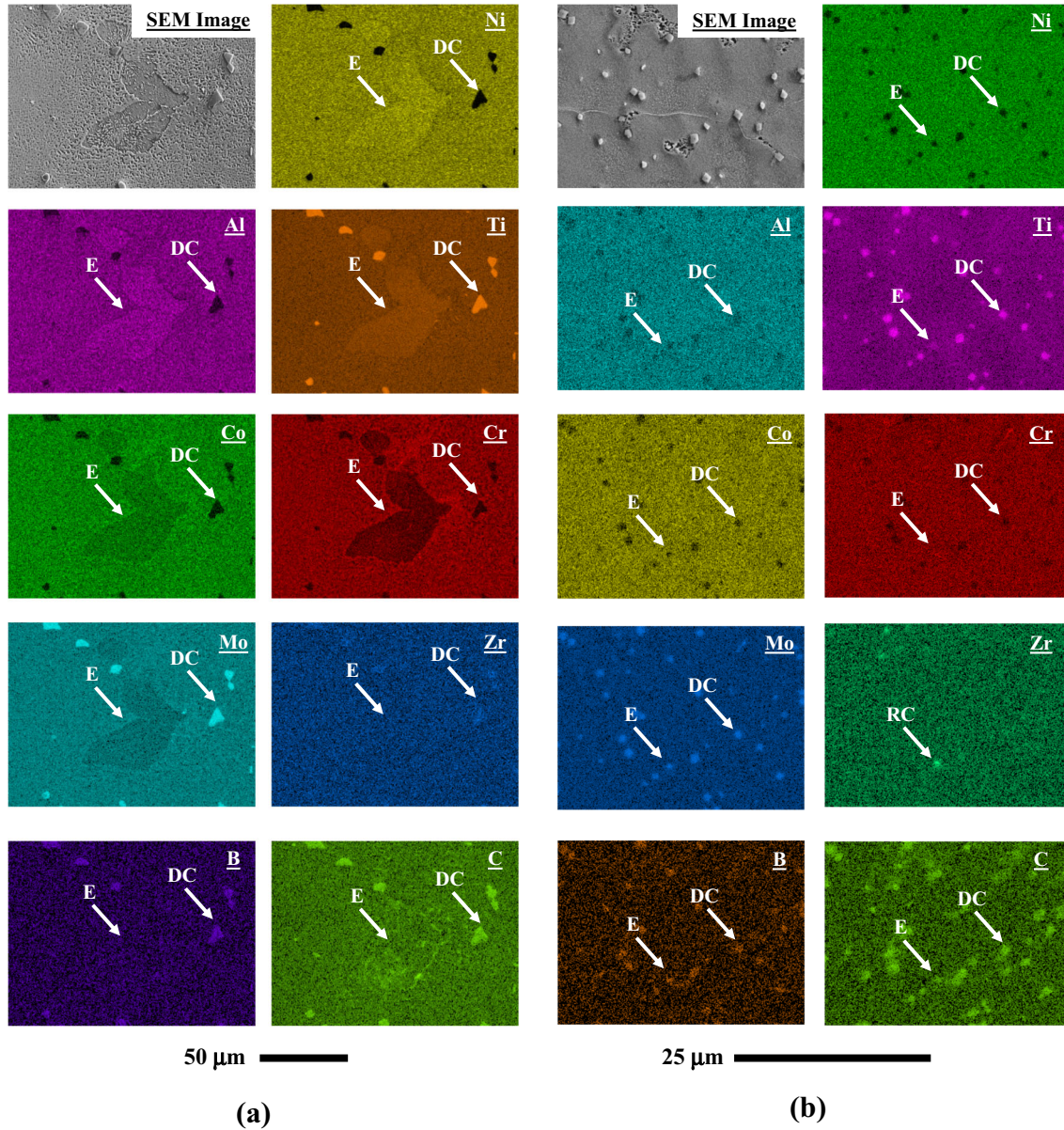


Fig. 3. Qualitative SEM-EDS elemental maps of a representative region in the (a) substrate and (b) deposit.

the pore count may be reduced by increasing the volumetric energy density by means of reducing the scan spacing, increasing the power, or reducing the scan speed.⁵ The microstructure of the as-deposited IN100 revealed the presence of columnar and equiaxed dendrites as shown in Fig. 1c. The deposit region showed a finer microstructure compared with the substrate region as shown in Fig. 1d. The microstructural refinement may be attributed to the localized heating and rapid cooling caused by the high-speed heat source. The microstructure of the deposited region revealed dendrite segregation patterns as shown in Fig. 1d.

In the present study, microhardness results indicated higher hardness values in the deposit region than in the substrate. Figure 1e shows three

different representative indentation marks in the deposit region. Figure 1f reports the average hardness values in the deposit, substrate, and interface regions of a representative IN100 sample. The average hardness value of the cast substrate was of order 390 ± 7 HV. The hardness increased to about 405 ± 11 HV near the interface region. The deposit region showed hardness values of order 430 ± 16 HV.

γ/γ' Microstructure

The major constituents of the microstructure of the SLE deposited IN100 were the γ matrix, the γ' precipitates in the γ matrix, the eutectics, and the carbide precipitates. Figure 2a and d illustrates the

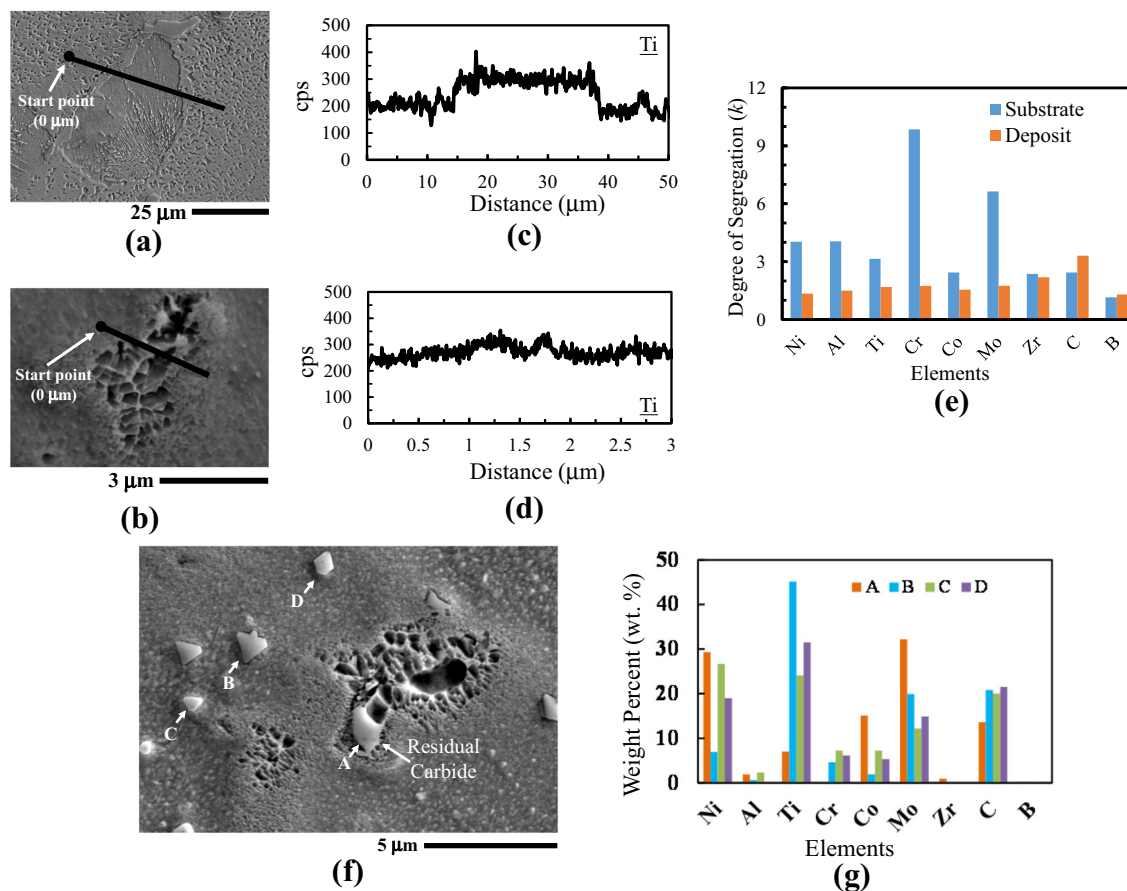


Fig. 4. SEM image of a representative line scan domain in the eutectic region of the (a) substrate and (b) deposit. EDS line profile of Ti across a representative eutectic region in the (c) substrate and (d) deposit. (e) Degree of segregation (k) of various alloying elements across representative eutectic pools in the substrate and the deposit. (f) SEM image of the carbide precipitates in the deposit region. (g) Composition of the carbide precipitates (in wt.%).

major constituents in the substrate and the deposit, respectively. In the deposit region, in addition to discrete carbide precipitates, a few residual carbide precipitates embedded in the eutectic pools were found as shown in Fig. 2d. The carbide precipitates were of order 50–200 nm in the deposit region, whereas in the substrate, they were of order 1–5 μm . As shown in Fig. 2b, the primary γ' precipitates showed a characteristic dimension in the range of 1–2 μm in the substrate region, whereas in the deposit region, the γ' precipitates were in the range of 50 nm as shown in Fig. 2e. Overall, the deposit region showed approximately 30 \times reduction in the γ' size compared with the substrate.

Figure 2c and f illustrates the γ/γ' morphology in the eutectic regions of the substrate and the deposit, respectively. The microstructures in Fig. 2c illustrate the irregular-shaped γ/γ' precipitates in the substrate eutectic region. The size of the eutectic regions was of order 25–75 μm in the substrate as shown in Fig. 2c. The finer cubic γ/γ' precipitates were of order 50–100 nm near the eutectic region in the deposit (Fig. 2f). The larger γ/γ' precipitates in

the deposit eutectic region were of order 200–400 nm as shown in Fig. 2f. The eutectic region in the deposits also showed a secondary γ/γ' microstructure with the γ' size in the range of 10–20 nm (Fig. 2f).

The microstructure of the substrate region showed significant changes after the SLE process was conducted. Figure 2g, h, and i shows the γ' structure in the post-SLE substrate at different locations (marked in Fig. 1b) along the direction of dominant thermal gradient i.e., [001]. At Location III, the γ' structure in the post-SLE substrate shows a similar size and shape compared with the substrate as shown in Fig. 2g and b, respectively. Here, the substrate and the post-SLE substrate reveal a bimodal γ' distribution with the primary γ' precipitates showing a characteristic dimension of order 1.5 μm and the secondary γ' precipitates showing a characteristic dimension of order 100 nm. At Locations II and I, however, the post-SLE substrate shows the collapse of larger γ' precipitates and moves from a bimodal distribution to a single mode distribution as a result of the heat effect during the SLE process.

Elemental Segregation

Figure 3a and b illustrates EDS maps of a representative region in the substrate and the deposit, respectively. Note that the eutectic region, the discrete carbide precipitates, and the residual carbide precipitates are marked by E, DC, and RC, respectively. In the substrate, Ni, Al, and Ti showed strong segregation to the eutectics. Co, Cr, and Mo showed strong segregation to the core (Fig. 3a). Ti, Mo, Zr, and B segregated to the carbides where Ni, Al, and Co were present in the carbide precipitates in trace amounts (Fig. 3a). C formed a rich layer along the periphery of the eutectic region in the substrate. In the deposit region, however, no elements showed strong segregation to the eutectics as shown in Fig. 3b. The carbide precipitates were uniformly distributed throughout the deposit region (Fig. 3b).

To characterize the elemental segregation in the eutectic regions, EDS line scans were performed across representative eutectic regions in the substrate and deposit, respectively (Fig. 4a and b). The line profiles of a representative element (Ti) across a eutectic region in the substrate and the deposit are shown in Fig. 4c and d, respectively. From the elemental line profiles, the maximum and the minimum counts were extracted and a segregation parameter was defined as *degree of segregation* (k) = *maximum cps/minimum cps* (where cps denotes counts per second). The k values for various elements are plotted in Fig. 4e for the substrate and the deposit regions. In comparison with the bulk alloy composition, the γ/γ' eutectic phase showed strong elemental segregation in the substrate, whereas in the deposit region, the degree of segregation was considerably lower.

IN100 contains about 0.18 wt.% C and 0.014 wt.% B resulting in the formation of carbide and boride precipitates in the deposit region. The blocky type of carbide precipitates was predominantly observed in the deposit region. The deposit region also showed a few residual carbide precipitates that were embedded in the eutectic pools as shown in Fig. 4f. Figure 4g illustrates the composition of four different carbide precipitates in the deposit region. The carbides were found to be rich in Ti, Ni, Mo, and Co; however, trace amounts of Cr and Al were also present. Zr only showed up in the residual carbide precipitates as shown in Fig. 4g, implying the presence of secondary solidification paths under rapid solidification conditions.¹⁷

CONCLUSION

The challenges associated with the processing of high- γ' nickel-base superalloys such as IN100 are well documented.^{3,4,15} Although this alloy has a high tendency for crack formation,⁴ in this work, crack-free, single-pass IN100 deposits having a deposit thickness of more than 1000 μm with length exceeding 35 mm and width exceeding 6 mm were obtained without preheating the powder bed.

Through optimization of the process parameters,⁵ the SLE process was demonstrated to be capable of ensuring a shallow melt-back depth of less than 100 μm . Such shallow melt-back depth lowers the probability of residual stress accumulation in the melt-back region and, therefore, crack formation. The high-resolution scan spacing used in the SLE process effectively preheats and provides post-heat treatment during the deposition process in-situ, reducing the possibility of hot tearing.

The SLE-fabricated microstructure was significantly finer than that in the investment cast substrate with the γ' precipitates showing approximately 30 \times reduction in size. The elemental segregation was also considerably lower in the deposit region. The superior microstructural uniformity in the as-built IN100 deposits may reduce the time required to homogenize the microstructure via heat treatment. The deposit region showed approximately 10% increase in the hardness values compared with the substrate. The findings obtained in this article thus demonstrate that the SLE process has a lot of potential in producing crack-free and complex parts of high- γ' nickel-base superalloys with exceptional microstructural properties.

In the future, detailed investigations will be performed on the SLE-deposited IN100 to assess the mechanical properties including tensile, creep, and shear strength. Heat treatment assessments will be performed, and the effects of heat-treatment on the microstructure and mechanical properties will be evaluated. Atom probe tomography (APT) will be carried out for an in-depth assessment of the composition and elemental partitioning of the constituent phases. The single-pass fabrication will also be extended to fabricate components through layer-by-layer AM.

ACKNOWLEDGEMENTS

This work was sponsored by the Office of Naval Research through Grant N00014-11-1-0670 as part of the Cyber-Enabled Manufacturing Systems (CeMS) program.

CONFLICT OF INTEREST

Dr. Suman Das is a co-founder of DDM Systems, a start-up company commercializing the SLE technology. Dr. Das and Georgia Tech are entitled to royalties derived from DDM Systems' sale of products related to the SLE research described in this article. This study could affect their personal financial status. The terms of this arrangement have been reviewed and approved by Georgia Tech in accordance with its conflict of interest policies.

REFERENCES

1. T.M. Pollock and S. Tin, *J. Propuls. Power* 22, 361 (2006).
2. M. Henderson, D. Arrell, R. Larsson, M. Heobel, and G. Marchant, *Sci. Technol. Weld. Join.* 9, 13 (2004).
3. A. Basak and S. Das, *Ann. Rev. Mater. Res.* 46, 125 (2016).

4. G. Bi, C.-N. Sun, H.-C. Chen, F.L. Ng, and C.C.K. Ma, *Mater. Des.* 60, 401 (2014).
5. R. Acharya and S. Das, *Metall. Mater. Trans. A* 46, 3864 (2015).
6. R. Acharya, R. Bansal, J.J. Gambone, M.A. Kaplan, G.E. Fuchs, N. Rudawski, and S. Das, *Adv. Eng. Mater.* 17, 942 (2015).
7. A. Basak and S. Das, *J. Alloys Compd.* 705, 806 (2017).
8. A. Basak and S. Das, *Mater. Sci. Forum* 879, 187 (2016).
9. R. Acharya, R. Bansal, J.J. Gambone, and S. Das, *Metall. Mater. Trans. B* 45, 2247 (2014).
10. R. Acharya, R. Bansal, J.J. Gambone, and S. Das, *Metall. Mater. Trans. B* 45, 2279 (2014).
11. A. Basak, R. Acharya, and S. Das, *Metall. Mater. Trans. A* 47, 3845 (2016).
12. A. Basak, S.H. Raghu, and S. Das, *J. Mater. Eng. Perform.* (2017). <https://doi.org/10.1007/s11665-017-3008-9>.
13. A. Basak and S. Das, in *Superalloys 2016*, ed. M. Hardy, E. Huron, U. Glatzel, B. Griffin, B. Lewis, C. Rae, V. Seetharaman, and S. Tin (Wiley, Hoboken, 2016), p. 1041.
14. A. Basak and S. Das, *Adv. Eng. Mater.* 19, 1600690 (2017). <https://doi.org/10.1002/adem.201600690>.
15. C. Körner, *Int. Mater. Rev.* 61, 361 (2016).
16. Nickel Institute, Engineering Properties of IN-100 Alloy, https://www.nickelinstitute.org/~media/Files/TechnicalLiterature/IN_100AlloyEngineeringProperties_483_.ashx. Accessed 8 Oct 2017.
17. Y.-J. Liang, J. Li, A. Li, X.-T. Pang, and H.-M. Wang, *Scr. Mater.* 127, 58 (2017).